Naval Research Laboratory
Washington, DC 20375-5320

NRL/6360/MR—2023/5

Synthesis of Hydrogen-Bond Donating UiO-66 Derivatives by Post-Synthetic Modification for Adsorption of Hazardous Chemicals

DANIEL A. CORBIN

National Research Council Research Associateship Program
Washington, DC

THOMAS C. CAO

American Society for Engineering Education Fellowship Program
Washington, DC

MICHAEL R. PAPANTONAKIS

VIET K. NGUYEN

CHRISTOPHER J. BRESHIKE

R. ANDREW MCGILL

Materials and Sensors Branch
Materials Science and Technology Division

October 10, 2023

REPORT DOCUMENTATION PAGE

Form Approved
OMB No. 0704-0188

1. REPORT DATE *(DD-MM-YYYY)*	**2. REPORT TYPE**	**3. DATES COVERED** *(From - To)*
10-10-2023	NRL Memorandum Report	

4. TITLE AND SUBTITLE

Synthesis of Hydrogen-Bond Donating UiO-66 Derivatives by Post-Synthetic Modification for Adsorption of Hazardous Chemicals

5a. CONTRACT NUMBER

5b. GRANT NUMBER

5c. PROGRAM ELEMENT NUMBER

6. AUTHOR(S)

Daniel A. Corbin*, Thomas C. Cao**, Michael R. Papantonakis, Viet K. Nguyen, Christopher J. Breshike, and R. Andrew McGill

5d. PROJECT NUMBER

5e. TASK NUMBER

5f. WORK UNIT NUMBER
1Y65

7. PERFORMING ORGANIZATION NAME(S) AND ADDRESS(ES)

Naval Research Laboratory
4555 Overlook Avenue, SW
Washington, DC 20375-5320

8. PERFORMING ORGANIZATION REPORT NUMBER

NRL/6360/MR--2023/5

9. SPONSORING / MONITORING AGENCY NAME(S) AND ADDRESS(ES)

10. SPONSOR / MONITOR'S ACRONYM(S)

11. SPONSOR / MONITOR'S REPORT NUMBER(S)

12. DISTRIBUTION / AVAILABILITY STATEMENT

DISTRIBUTION STATEMENT A: Approved for public release; distribution is unlimited.

13. SUPPLEMENTARY NOTES

*National Research Council Research Associateship Program, Washington, DC
**American Society for Engineering Education Fellowship Program, Washington, DC

14. ABSTRACT

New metal-organic framework (MOF) sorbents are developed based on the UiO-66 series as a scaffold for grafted sorbent moieties. Post-synthetic modification of UiO-66-NH2 is performed via condensation reactions with benzaldehyde and benzoic acid derivatives to install hydrogen-bond donating groups within the framework. Analysis performed by nuclear magnetic resonance spectroscopy to characterize the digested MOFs supports successful linker functionalization. The effects of varying the electronic properties of MOF substituents (i.e. electron-donating and electron-withdrawing) on sorbent properties are investigated. Most notably, incorporation of functional groups into the MOFs is shown to benefit sorbate uptake capacity and increase sorbent binding affinity for targeted chemicals, demonstrating the viability of this approach to sorbent design. However, beneficial design criteria may not be universal and may vary by functionalization approach, suggesting each system must be carefully studied to optimize sorbent performance.

15. SUBJECT TERMS

Metal-organic framework, MOF, Adsorbent, Sorbent, Sorbate, Hydrogen-bonding, Post-synthetic modification, Organophosphate, COLPRO

16. SECURITY CLASSIFICATION OF:			**17. LIMITATION OF ABSTRACT**	**18. NUMBER OF PAGES**	**19a. NAME OF RESPONSIBLE PERSON**
					Daniel Corbin
a. REPORT	**b. ABSTRACT**	**c. THIS PAGE**			**19b. TELEPHONE NUMBER** *(include area code)*
U	U	U	U	23	(202) 767-6302

Standard Form 298 (Rev. 8-98)
Prescribed by ANSI Std. Z39.18

This page intentionally left blank.

CONTENTS

This page intentionally left blank.

SYNTHESIS OF HYDROGEN-BOND DONATING UIO-66 DERIVATIVES BY POST-SYNTHETIC MODIFICATION FOR ADSORPTION OF HAZARDOUS CHEMICALS

INTRODUCTION

The development of protection technologies to prevent human exposure to hazardous chemicals is beneficial to the Navy and all DOD services, as well as a variety of civilian applications related to chemical manufacturing and first responder communities [1]. A crucial component of these technologies is the sorbent [2], which serves as a molecular and particulate filter to remove chemicals from air and water. While there are countless examples of hazardous chemicals in existence, they can be organized into categories according to their chemical properties. For example, chlorine and phosgene can be classified as acidic or acid-forming chemicals [2], while common solvents such as benzene, xylene, methanol, acetone fall in the class of volatile organic compounds [3]. In this work, our interest is basic and hydrogen-bond accepting chemicals, such as organophosphates [2,4,5] and ammonia [3,6,7], which present hazards across DOD and civilian applications.

Previous work designing sorbents for these chemicals, as well as others, has emphasized the use of activated carbon as the primary sorbent material. One advantage of activated carbon is that it offers broad protection against a variety of hazardous chemicals, since binding occurs through non-specific dispersion forces within the channels and pores of the material [2,6,8]. However, these materials show limitations that should be addressed by future sorbent designs. For example, very small and highly polar molecules (e.g. ammonia) are poorly bound by activated carbon, significantly reducing sorbent capacity [9]. In addition, the performance of activated carbons is known to decrease during exposure to high humidity [6,10] due to water condensation within the pores of the sorbent, limiting their utility in certain environments. From a research perspective, these materials are also difficult to study due to their irregular and poorly defined structures, which make performing systematic investigations challenging [8].

More recently, metal-organic frameworks (MOFs) have gained significant attention as platforms for both physical removal of hazardous chemical sorbents [2,3,6–8] and as catalysts for the degradation of these hazardous chemicals [3,11]. Perhaps the first example exploring MOFs in such applications came from Ni *et al.* in 2007, where IRMOF-1 was shown to bind dimethyl methylphosphonate (DMMP) effectively and in a selective fashion [12]. Shortly thereafter, Britt *et al.* compared the gas adsorption performance of several isoreticular MOFs to that of a common activated carbon, showing that in many cases MOFs can exhibit superior adsorption to traditional carbon-based sorbents [13]. Despite these exciting discoveries, early MOF sorbents suffered from poor stability under ambient atmospheric conditions [12]. Since hydrolysis of metal-oxygen bonds within the framework was a suspected cause of this instability, subsequent work focused on developing hydrophobic MOFs that could minimize undesirable interactions with atmospheric water [14–16]. More recently, research has investigated MOFs with more inherent chemical stability, such as UiO-66 [17,18] and other Zr-based MOFs [3].

Separately, polymeric sorbents have been studied for use as sensor coatings to selectively bind target chemistries and in preconcentrator devices for hazardous chemical sensing applications. One early sorbent developed at the NRL is fluoropolyol (FPOL, Fig. 1) [19], which was later employed as an active layer for organophosphate binding within surface acoustic wave sensors [20–23]. Following the success of this sorbent, we became interested in developing new materials that could improve upon the performance of FPOL. As a result,

Manuscript approved October 6, 2023.

several new materials were introduced, including novel polymeric sorbents (Fig. 1) [24,25] and small molecule analogues [26,27]. While many of these absorbent materials have shown improvements in sorbent performance relative to FPOL, such as increased binding affinity for DMMP, they suffer from several limitations. Due to the flexibility of the polymer chains, sorbent hydroxyl groups, which are primarily responsible for hydrogen-bonding to hazardous chemicals, exhibit self-association interactions that can interfere with binding of target chemicals [27]. More importantly, the application of these materials in protection equipment is hindered by their non-porous nature, which limits hazardous chemical binding to the surface of the sorbent or through slow absorption processes into the "bulk" absorbent material.

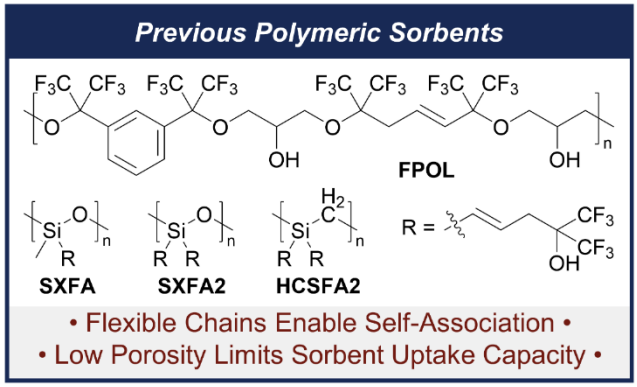

Fig. 1—Previous polymeric sorbents and the limitations of these materials

To address these limitations, we envisioned applying the design principles developed for polymeric and small molecule absorbents to a MOF architecture. As such, this work explores the post-synthetic modification (PSM) of well-established MOFs by adding sorbent moieties to augment their capabilities against hazardous chemicals (Fig. 2). The PSM strategy was selected for its ability to introduce a range of functional groups into MOFs without compromising the underlying MOF structure [28–34]. By selecting a parent MOF that displays chemical stability on its own, this approach allows for rapid generation of new materials that can withstand the challenging conditions of these protection applications. Specifically, the UiO-66 series was selected for its excellent chemical stability [35–39] and ability to be post-synthetically modified [29,30]. Following PSM, structural characterization of the resulting f-MOFs was performed prior to testing sorbent capabilities. DMMP was chosen as the target sorbate chemical for these studies given the previous use of this chemical in the literature [2,6,8,12,20,23,25,27]. By introducing sorbent moieties with varying electronic properties, structure-property relationships are discovered that may guide future investigations and sorbent design.

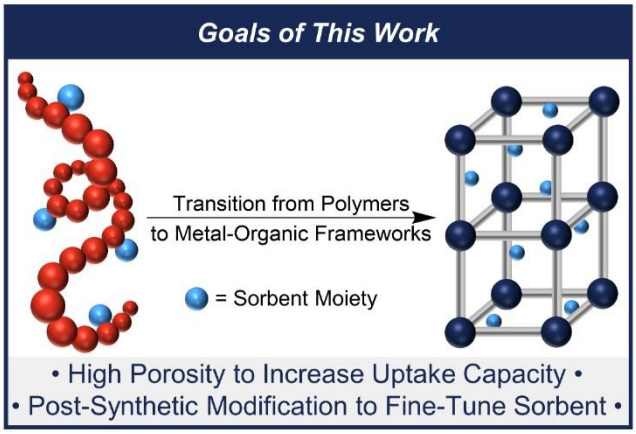

Fig. 2—The central goal of this work: develop porous MOF sorbents with tunability to understand how structure impacts sorbent performance

EXPERIMENTAL

Chemical Sources and Storage

All reagents were obtained from either Sigma Aldrich or Ambeed and used as received. All manipulations were carried out in a standard laboratory fume hood under ambient atmosphere. MOFs were stored under ambient conditions and dried thoroughly prior to analysis by drying overnight at 120 or 200 °C under reduced pressure.

Instrumentation

Infrared (IR) spectroscopy was performed on a Bruker Vertex 80v FT-IR spectrometer with a PIKE Technologies MIRacle Single Reflection attenuated total reflectance (ATR) attachment equipped with a diamond crystal. Spectra were collected under vacuum and background corrected. Nuclear magnetic resonance (NMR) spectra were collected on a Bruker Ascend spectrometer (400 MHz) and are reported in parts per million (ppm, δ). ^{1}H NMR spectra are referenced to the residual solvent peak at 4.79 ppm for D_2O. Powder x-ray diffraction data was collected on a Rigaku SmartLab powder diffraction system equipped with a D/tex ultra 1D detector and a Cu x-ray source using a Bragg-Brentano geometry. Nitrogen gas adsorption measurements were performed on a Micromeritics Tristar II Plus at 77K. Samples were activated prior to measurement on a Micromeritics Smart VacPrep system by heating at 200 °C under vacuum for 8h.

Vapor uptake studies were performed using a Biolin Scientific QSense Analyzer quartz crystal microbalance (QCM) and a custom NRL developed vapor generation system. Vapor generation was achieved by flowing nitrogen through the head-space above liquid DMMP (for uptake studies) and bubbling nitrogen through liquid DMMP (for Henry's Law studies). The temperature of the DMMP was maintained at 25 °C (for uptake studies) or 20 °C (for Henry's Law studies) using a thermostated oil or water bath. Initially, the vapor stream was sent to waste until sufficient time had passed to achieve a steady flow of the target vapor. During this period, the QCM response was stabilized under a constant flow of dry air. The gas stream was then switched to deliver the desired vapor stream to the QCM system. The temperature of the QCM system was maintained at 25 °C during all experiments. After each experiment, the gas flow was switched back to dry air. In every case, a constant flow rate was maintained using an Apex mass flow controller. Since the QSense Analyzer allows for four simultaneous QCM measurements, the gas inlet line was split four ways to deliver vapor to the four QCM cells in parallel.

General Procedure for MOF Functionalization.

UiO-66-NH_2 was synthetized according to a literature procedure [37]. A single, multi-gram batch was synthesized and used for all subsequent modifications to eliminate batch-to-batch variations that might influence sorbent performance.

UiO-66-NH_2 was functionalized according to a modified literature procedure [40,41]. UiO-66-NH_2 (200 mg) was weighed into a 20 mL glass scintillation vial. The quantity of amine-groups in this amount of UiO-66-NH_2 was approximated based on the mass-ratio of -NH_2 to an ideal MOF formula unit [$Zr_6O_4(OH)_4$(BDC-NH_2)$_6$, where BDC-NH_2 = 2-amino-1,4-benzenedicarboxylate]. The mass of -NH_2 in 200 mg UiO-66-NH_2 was then converted to moles (0.684 mmol, 1 eq). For each functionalization reaction, the chosen coupling partner was weighed and added to the reaction vial (1.368 mmol, 2 eq), along with methanol (10 mL) and a magnetic stir-bar. The reaction was stirred at room temperature for 7 days, after which the product was collected by vacuum filtration and washed with

clean methanol (4 x 10 mL). The product was dried briefly under air before being left to dry further in a vacuum oven at 120 °C for several days.

In some cases, residual coupling partner in the functionalized MOF could be observed by ^{1}H NMR after suspending the MOF in D_2O for 30 minutes. For each sample where this impurity was found, the functionalized MOF was soaked in methanol overnight, filtered, and dried again as described above. In most cases, this procedure was sufficient to remove all detectable residual coupling partner.

General Procedure for MOF Digestion.

A small quantity of MOF (~ 2 – 5 mg) was added to an NMR tube along with 0.4 mL of saturated $NaHCO_3$ in D_2O. The solution was mixed vigorously and allowed to react for 30 minutes. In most cases, the solution changed from colorless to lightly colored (typically yellow or orange), and some solid remained in the bottom of the NMR tube. The solution was immediately characterized by NMR spectroscopy.

RESULTS AND DISCUSSION

Unmodified MOFs (UiO-66, UiO-66-OH, and UiO-66-NH_2) were synthesized according to the procedure reported by Katz and Brown *et al.* using $ZrCl_4$, the corresponding dicarboxylate linker, *N,N*-dimethylformamide as the reaction solvent, and concentrated hydrochloric acid as a modulator [37]. The MOFs UiO-66 and UiO-66-OH were chosen as control systems, since UiO-66 does not feature any specific sorbent moiety while UiO-66-OH has a hydroxyl group on every linker. The MOF UiO-66-NH_2 was chosen for further modification since many published PSM strategies rely on the reactivity of amine groups within the MOF [28–30,40–46]. To increase confidence that differences in sorbent performance can be attributed to the sorbent groups installed in the framework, UiO-66-NH_2 was synthetized on a multi-gram scale such that all modifications could be made to a single batch of material.

As this work targets the adsorption of hydrogen-bond-accepting hazardous chemicals, a PSM method was sought to install hydroxyl-bearing groups that could act as good hydrogen-bond donors. In addition, the ability to install other functional groups that could tune the -OH acidity was desired, such that structure-property relationships could be investigated in this new class of adsorbents. Specifically, electron withdrawing groups of varying strength (CF_3 and F) and electron donating groups (OMe) were incorporated to investigate the impact of these electronic modulating groups on sorbent performance.

Two approaches to PSM were explored: condensation of benzaldehydes [40,41] to form f-MOFs with imine-bridges between the MOF linker and the grafted sorbent group (imine series: Fig. 3, left), and condensation of benzoic acids [46] to form f-MOFs with amide-bridges (amide series: Fig. 3, right). While previous reports employed toluene as the reaction solvent [40,41], methanol was chosen in this work due to the favorable solubility of the benzaldehyde and benzoic acid coupling partners. In nearly every case, f-MOFs exhibited a characteristic color change [40,41,46] over time from light yellow to dark yellow or orange, consistent with successful functionalization of the MOF.

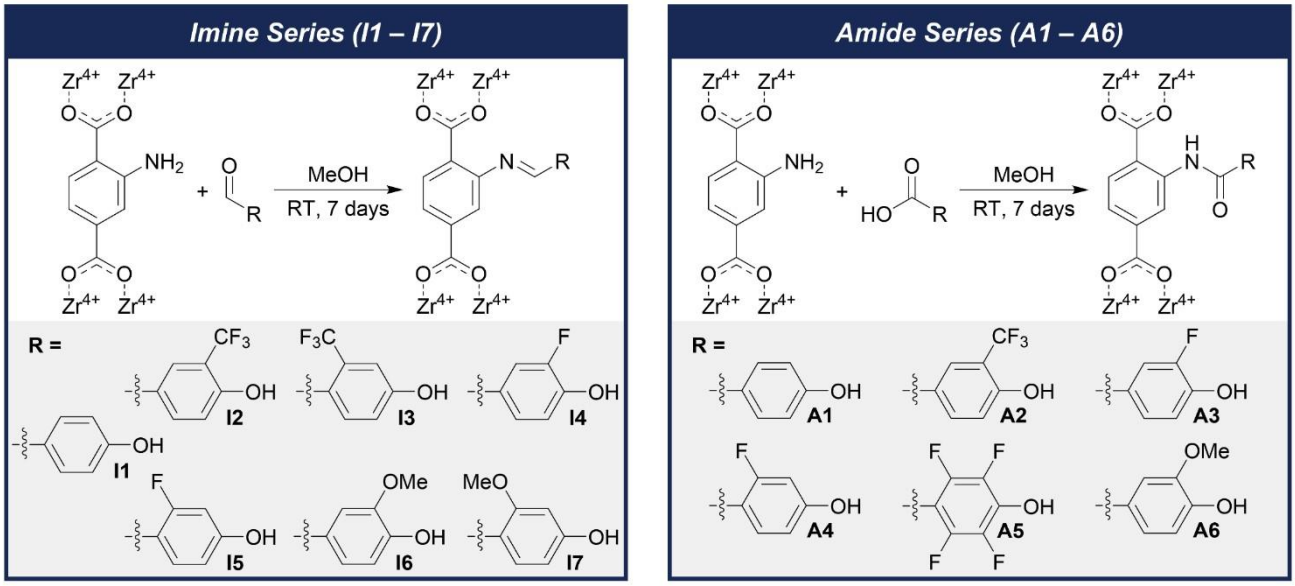

Fig. 3—General reaction schemes for the functionalization of MOFs in this work. Coupling partners include benzaldehydes to generate imine functionalized MOFs (left) and benzoic acids to generate amide functionalized MOFs (right)

Functionalized MOFs were initially characterized using attenuated-total-reflectance infrared (ATR-IR) spectroscopy to probe for the presence of residual coupling partner. In every case, the f-MOF IR spectra (Appendix A, Figs. A1 – A2) showed complete removal of the free coupling partner as a result of post-modification washing with excess methanol. The IR spectra were also analyzed for possible new signals corresponding to imine or amide stretches that could support successful MOF functionalization, but no obvious assignments could be made.

To gain better insight into the products of the functionalization reactions, f-MOFs were digested and their free linkers were characterized by nuclear magnetic resonance (NMR) spectroscopy. While UiO-66 MOFs are often digested using hydrofluoric acid [30,43,45,47], this approach was avoided due to the catalytic role acids can play in the hydrolysis of imines and amides [48]. Instead, more mild digestion conditions [49] were chosen employing $NaHCO_3$ (Fig. 4) to preserve connectivity between the MOF linkers and added sorbent groups. The digested solutions (dark blue traces) were then compared to UiO-66-NH_2 digested under the same conditions (light blue) and the free coupling partner in the same saturated $NaHCO_3$ / D_2O solution (red).

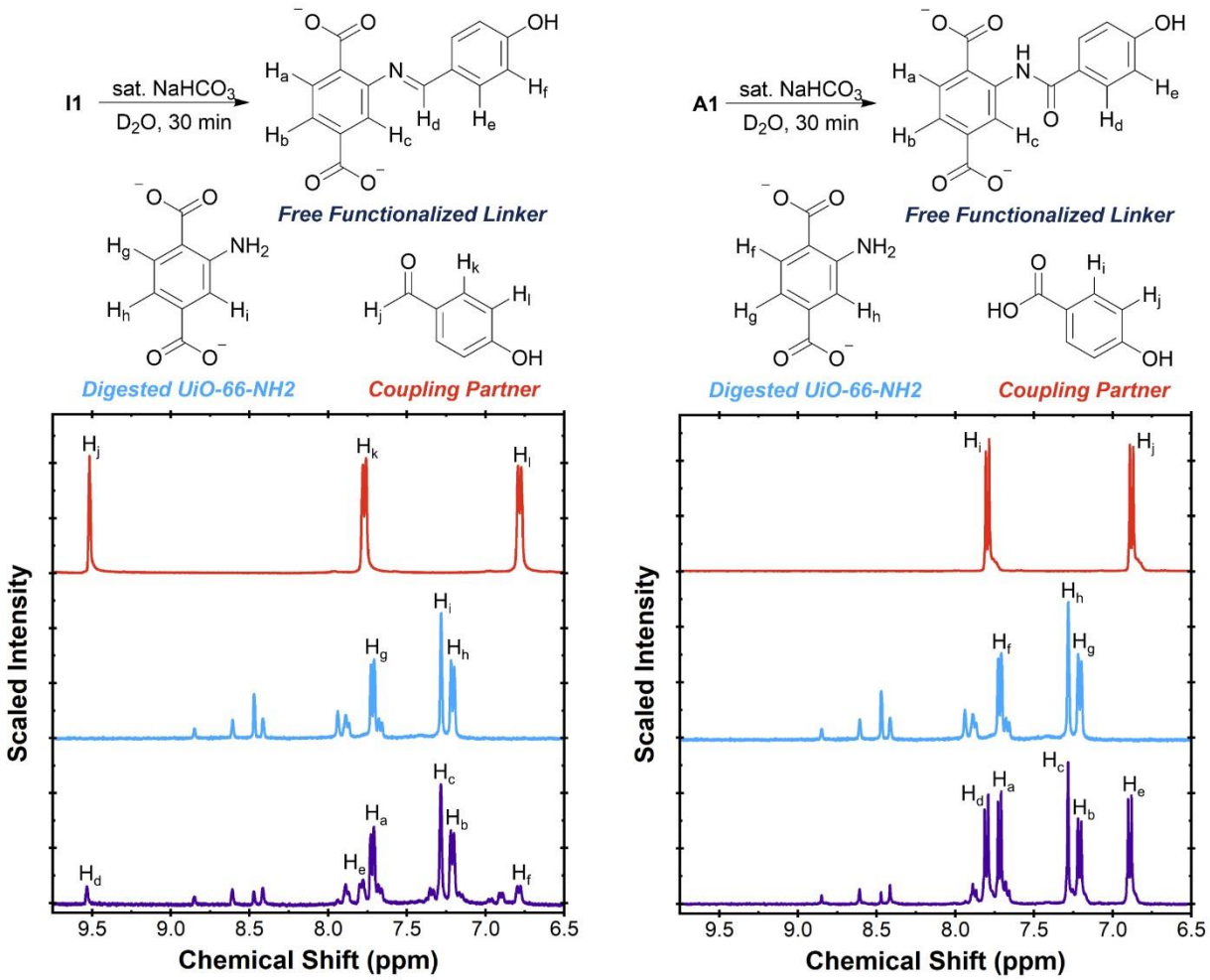

Fig. 4—Digestion of **I1** (left) and **A1** (right) in saturated $NaHCO_3$ and its resulting ^1H NMR spectra (dark blue). The spectra of digested UiO-66-NH_2 (light blue) and 4-hydroxybenzaldehyde or 4-hydroxybenzoic acid coupling partner in the presence of saturated $NaHCO_3$ (red) are provided for reference

In each case, peaks were observed corresponding to the unfunctionalized BDC-NH_2 linker as well as the added sorbent moiety. Slight changes in the chemical shifts of the sorbent group signals relative to the free coupling partners suggest successful attachment of these groups to the MOF linkers, since attachment to the linkers should perturb the electronic properties of the sorbent groups to some degree. Alternatively, it is possible the signals assigned here to the attached sorbent groups could in fact be residual coupling partner left over from the functionalization reactions. To test this possibility, f-MOF samples were also soaked in D_2O and analyzed by NMR spectroscopy to probe for the presence of unbound, soluble impurities. In each case, little-to-no residual coupling partner could be observed, suggesting the signals observed in the f-MOF digestions are in fact due to the functionalized linkers. Using the ^1H NMR spectra of the digested f-MOFs, the percentage of linkers functionalized was estimated based on the relative peak integrations for the sorbent moieties (i.e. the bound coupling partner) and the unfunctionalized BDC-NH_2 linkers. The values obtained are provided in Table 1. In general, the amide series showed greater incorporation of sorbent groups than the imine series, with the percent of linkers functionalized appearing consistently around 50%. For the imine series, electron-rich sorbent groups (**I6** and **I7**) produce higher degrees of incorporation (~ 20%) than electron-neutral or electron-deficient groups (~ 5%). However, it is unclear why this phenomenon is observed.

Table 1—Characterization data for UiO-66, UiO-66-NH_2, UiO-66-OH, **I1** – **I7**, and **A1** – **A6**

Sorbent	% Functionalized [a]	SA_{BET} [b] (m^2 g^{-1})	Uptake Capacity [c] (mmol g^{-1}) [d]	Normalized Capacity (μmol m^{-2}) [e]
UiO-66	-	1360 ± 30	0.123 ± 0.013	0.090 ± 0.010
UiO-66-NH_2	0	1080 ± 120	0.137 ± 0.068	0.126 ± 0.063
UiO-66-OH	-	310 ± 60	0.124 ± 0.016	0.401 ± 0.051
I1	5	420 ± 40	0.084 ± 0.003	0.199 ± 0.007
I2	5	640 ± 40	0.104 ± 0.006	0.163 ± 0.009
I3	2	500 ± 50	0.315 ± 0.035	0.630 ± 0.070
I4	6	570 ± 10	0.144 ± 0.018	0.252 ± 0.032
I5	6	530 ± 20	0.109 ± 0.028	0.205 ± 0.053
I6	23	640 ± 70	0.028 ± 0.004	0.043 ± 0.006
I7	18	470 ± 40	0.144 ± 0.033	0.306 ± 0.071
A1	49	160 ± 20	0.055 ± 0.013	0.341 ± 0.079
A2	18	680 ± 20	0.058 ± 0.002	0.085 ± 0.003
A3	52	240 ± 90	0.075 ± 0.013	0.313 ± 0.053
A4	55	230 ± 10	0.049 ± 0.002	0.214 ± 0.010
A5	- [f]	470 ± 20	0.124 ± 0.003	0.264 ± 0.005
A6	65	140 ± 30	0.108 ± 0.041	0.769 ± 0.296

[a] Determined by ^1H NMR based on the quantity of coupling partner incorporated relative to free BDC-NH_2.
[b] Brunauer-Emmett-Teller surface area determined by nitrogen gas adsorption at 77K; measurements performed in triplicate.
[c] Uptake capacity of DMMP measured at 25 °C on samples dried in a vacuum oven at 120 °C; measurements performed in triplicate.
[d] Uptake capacity reported as mmol of DMMP per gram of sorbent.
[e] Normalized capacity refers to the uptake capacity divided by the surface area of the sorbent and is reported as μmol of DMMP per m^2 of the sorbent.
[f] Percent of functionalization could not be obtained for **A5** due to the lack of observable protons for this coupling partner.

Analysis of the f-MOFs by powder x-ray diffraction revealed many of the functionalized materials exhibit a loss of crystallinity, as indicated by peak broadening in the powder patterns (Appendix A, Fig. A3). Similar observations have been reported by others following UiO-66 exposure to methanol, which is believed to facilitate linker exchange by interrupting bonding between MOF linkers and nodes [50]. Despite this peak broadening, the same general features were observed as in the powder patterns of UiO-66 and UiO-66-NH_2, indicating some preservation of the framework structure.

To evaluate whether this loss of crystallinity is detrimental to MOF surface area, N_2 gas adsorption was performed. The resulting data was analyzed according to Brunauer-Emmett-Teller (BET) theory [51– 54] using the fitting criteria described by Rouquerol [55]. All of the f-MOFs investigated in this work exhibited Type I isotherms [52,53] similar to the unfunctionalized MOFs (Appendix A, Figs. A4 – A6). Further, all of the f-MOFs displayed lower surface areas than unfunctionalized UiO-66-NH_2 (Table 1), which is consistent with incorporation of the sorbent groups within the framework. For materials with greater sorbent group incorporation (~ 50%), a weak correlation is observed between the percentage of functionalized linkers and f-MOF surface area (Fig. 5). However, materials with fewer sorbent groups (~ 5 – 20%) show no correlation, as all these materials have roughly half the surface area of the unfunctionalized UiO-66-NH_2 starting material. While the reason for this observation is not clear,

it could be related to the large number of defect sites created during MOF synthesis [37] or perhaps the reduced crystallinity of these materials following PSM. However, further investigation is necessary to understand how each of these variables might impact the surface area of the final material.

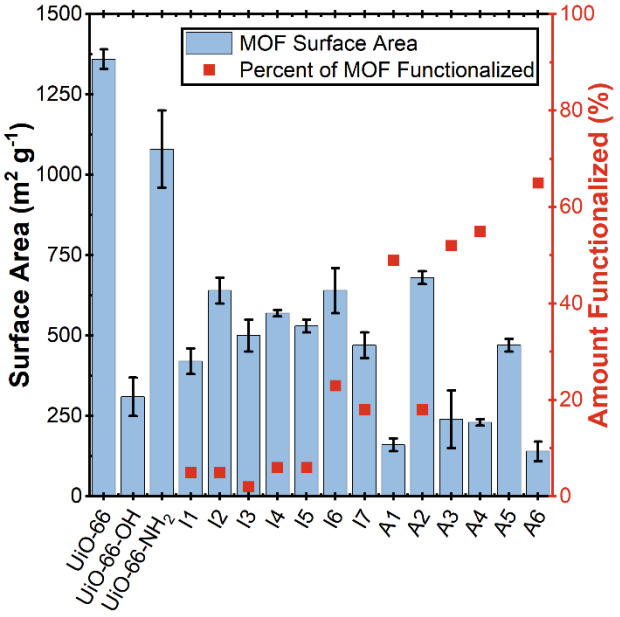

Fig. 5—Comparison of MOF surface areas (blue bars) as measured by N_2 gas adsorption relative to the amount of the MOF that was functionalized (red points). Measurements were performed in triplicate; error bars represent the standard deviation from three measurements

It is important to note that the activated carbons that are commonly used as adsorbents in protection applications typically exhibit surface areas ranging from about 500 – 1500 m^2 g^{-1} [56,57]. Thus, the f-MOFs developed in this work should be suitable for use in similar protection applications. With that said, greater surface areas would certainly be beneficial, and MOFs have been reported with surface areas as high as 7300 m^2 g^{-1} [58], highlighting the potential of this class of materials.

To probe whether these f-MOFs could function as adsorbents for hazardous chemicals, the uptake capacity of these materials (Table 1) was measured using a quartz crystal microbalance (QCM) testbed. Gold-coated QCM sensors were obtained, cleaned, and measured to determine their uncoated oscillation frequencies. Suspensions of each f-MOF were then prepared in ethanol and drop-cast separately onto the sensors. After thorough drying in a vacuum oven for several days, the sensors' oscillation frequencies were remeasured to determine the mass of each f-MOF deposited on the sensor surface. A stream of saturated DMMP in dry air was then passed over the surface of the sensors, causing the oscillation frequency of each sensor to change as DMMP adsorbed in the MOFs. Saturation of the MOFs was assumed once the sensors' oscillation frequencies stabilized, allowing for calculation of each material's DMMP uptake capacity based on the amount of DMMP adsorbed per mass of sorbent.

At first glance, functionalization with various sorbent groups appears to have a limited, if not negative, impact on uptake capacity (Fig. 6, blue bars). In nearly every case, the unfunctionalized MOFs UiO-66 and UiO-66-NH_2 exhibit similar or even better uptake capacities relative to the f-MOFs developed in this work. However, it is important to consider the impact of surface area on these measurements, as uptake capacity is expected to be directly related to the available surface area of each MOF. Since the f-MOFs developed here show decreased surface areas as a result of functionalization, some decrease in overall capacity is not surprising. Therefore, to focus on just the impact of these added functionalities on sorbent performance, the data was normalized to the surface area of

each material (Fig. 6, red bars). In the future, this limitation can easily be addressed by functionalizing MOFs with larger pores, which would increase the surface area of the final material and limit the effect of the added sorbent group on porosity.

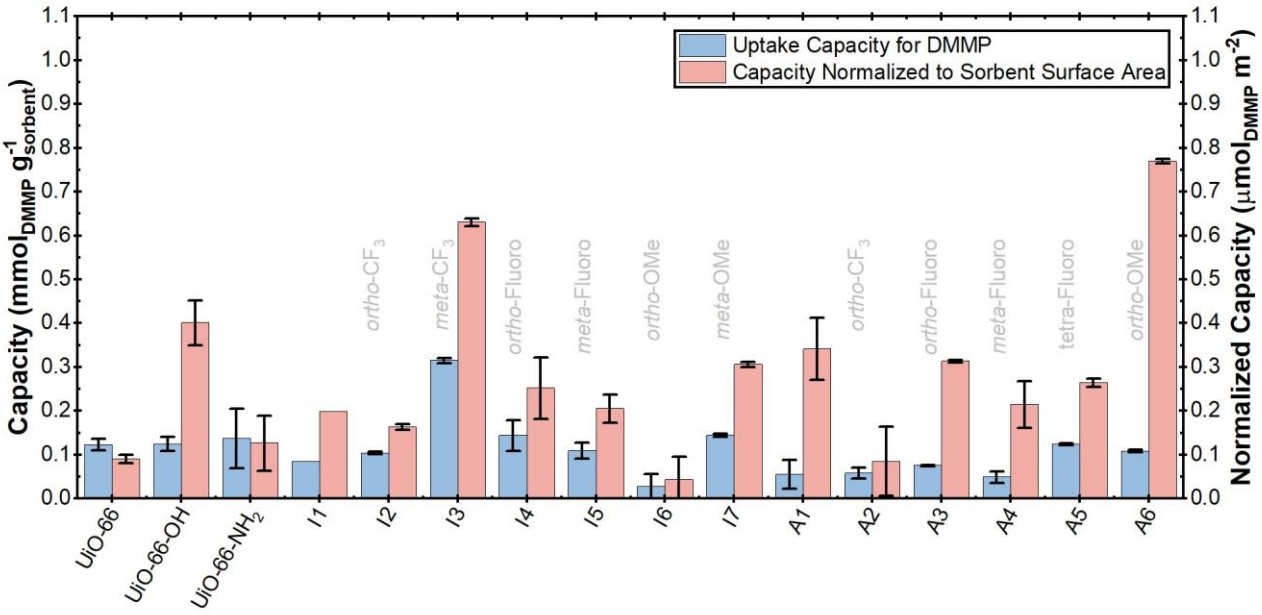

Fig. 6—Measurement of sorbent uptake capacity for DMMP using a QCM testbed. Capacity is displayed versus sorbent weight (blue bars) and sorbent surface area (red bars). For samples in which functional groups are defined (light grey text), positions are relative to the hydroxyl group

Considering the data in this manner, a few interesting observations can be made. In many cases, the f-MOFs show improved normalized uptake capacity for DMMP relative to UiO-66 and UiO-66-NH_2. This observation agrees with expected trends and indicates that the added sorbent groups enable more DMMP to be adsorbed relative the unfunctionalized MOFs, absent any contributions from the surface area of the MOF. In addition, UiO-66-OH is among the materials with the highest normalized uptake capacities, likely due to the high concentration of hydroxyl groups that can act as sorbent sites within the MOF.

Perhaps the most interesting discovery was the correlation of normalized uptake capacity with the Hammett constants of the electron-donating and electron-withdrawing substituents within the sorbents. Hammett substituent constants were originally developed to understand the effects of aromatic substituents on the ionization of benzoic acid derivatives [59]. Since then, they have been used to understand equilibrium processes, reaction kinetics [60], and even non-covalent interactions [61]. In this work, the normalized uptake capacity of each f-MOF was plotted versus the respective Hammett constant to gain insight into how substituent electronic effects and positions relative to the hydroxyl group impact sorbent performance. Since Hammett constants for *ortho*-substituents are often ignored due to possible steric interference, these values were estimated from the respective *para*-substituent constants in accordance with a previous report ($\sigma_o \sim 0.75*\sigma_p$) [62].

In the case of the imine series, a positive correlation was observed between the Hammett substituent constants and normalized uptake capacity (Fig. 7, left). This correlation reveals that in imine-functionalized MOFs, electron-withdrawing substituents are most beneficial for sorbent capacity. In addition, the position of the substituent also plays an important role, since the electronic impact of the substituent in the *ortho*, *meta*, and *para* positions varies due to changes in resonance and inductive effects. Importantly, two outliers were omitted from this

analysis – **I2** and **I5**. In the case of **I2**, deviation from the expected trend is not surprising given that the *ortho*-CF_3 group may cause steric interference during DMMP binding, an effect that is not considered by Hammett constants. Instead for **I5**, it is not clear why this sample does not follow the trend observed with the other materials in this series.

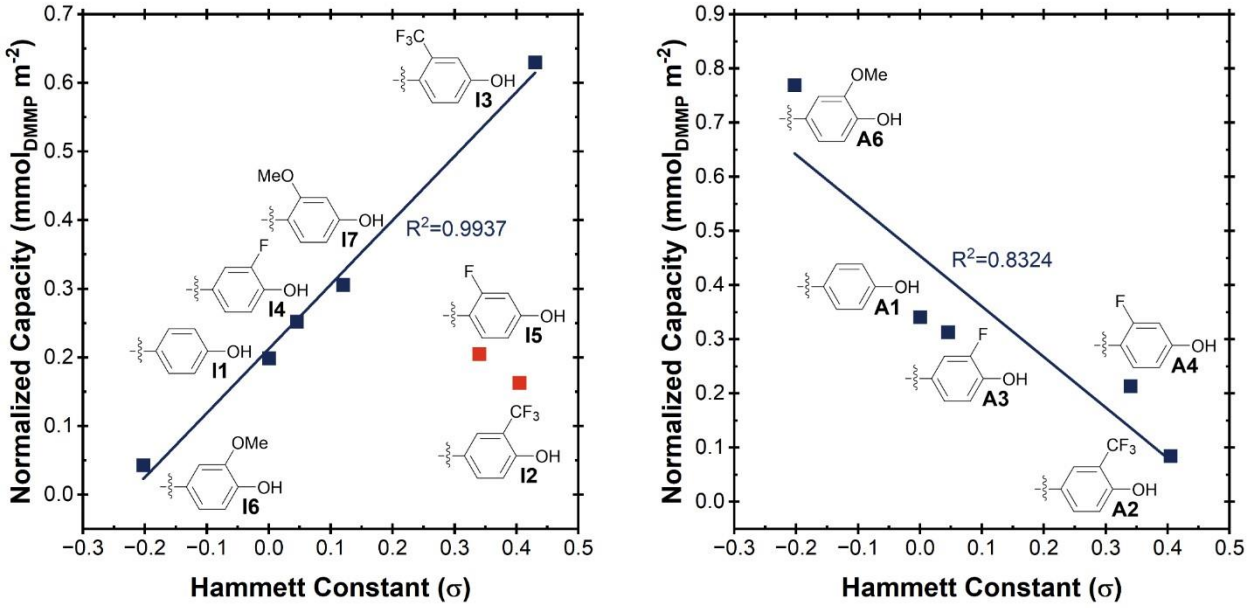

Fig. 7—Correlation of normalized sorbent capacity with Hammett constants for the imine series (left) and amide series (right) of sorbents. Outliers are displayed in red. For *ortho*-substituents, σ_o was calculated as $0.75*\sigma_p$ (the Hammett constant for the same substituent in the *para*-position) [62]

Unexpectedly, the amide series shows the opposite trend of the imine series (Fig. 7, right). In this case, normalized uptake capacity is negatively correlated with the Hammett substituent constants, indicating that electron-donating groups may be most beneficial for sorbent performance in this series. This discovery is surprising and indicates a fundamental difference between the imine- and amide-functionalized sorbents, although the cause of this difference is unclear at this time.

In an attempt to understand these observed differences between the imine- and amide-functionalized MOFs, the binding affinities of each sorbent were analyzed using the same QCM apparatus described above. This time, instead of a saturated DMMP vapor stream, a diluted vapor stream was employed with [DMMP] ranging from ~50 to 1000 parts per billion. At each [DMMP], the quantity of DMMP adsorbed was calculated and converted to the [DMMP] within the sorbent ($[DMMP]_{ads}$). This value was then divided by the [DMMP] in the vapor phase ($[DMMP]_{vapor}$) to give $\log(K_H)$ at each point, where $K_H = [DMMP]_{ads} / [DMMP]_{vapor}$. By performing this analysis at various $[DMMP]_{vapor}$ and applying a linear regression to infinite dilution (i.e. $[DMMP]_{vapor} = 0$, or the y-intercept of the $\log(K_H)$ vs. $[DMMP]_{vapor}$ plot), the limiting value of $\log(K_H)$, or the Henry's Law binding constant, was obtained.

Figure 8 shows the results of these analyses, which demonstrates an improvement in binding affinity for DMMP [i.e. an increase in $\log(K_H)$] for all functionalized MOFs relative to the unfunctionalized UiO-66-NH_2 precursor. Unfortunately, attempts to correlate these data to Hammett substituent constants as was done previously were unsuccessful, suggesting the binding affinity of each sorbent group cannot explain the structure-property relationships observed for uptake capacity. However, these results do exhibit a broad correlation with each material's degree of functionalization (Appendix A, Fig. A7), highlighting the importance of maximizing functionalization

through the chosen PSM approach. It is also interesting to note that UiO-66-OH shows one of the strongest affinities for DMMP of all the sorbents tested in this work despite no further functionalization being performed on this material.

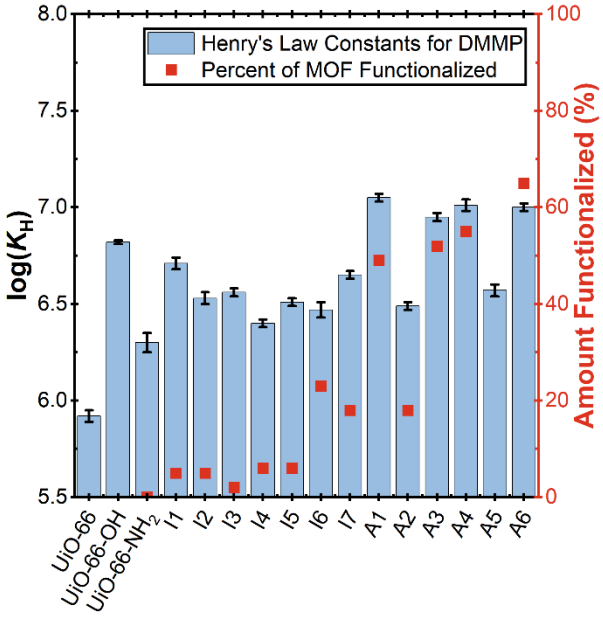

Fig. 8—Henry's Law binding constants for imine- and amide-functionalized f-MOFs relative to their degree of functionalization

In addition to their binding affinities for DMMP, it is important to consider how these sorbents interact with other chemicals that might interfere with DMMP adsorption. In an attempt to quantify possible interfering effects, a similar Henry's Law study was performed using toluene instead of DMMP. Table 2 compares the results of these measurements with those using DMMP, highlighting that UiO-66-OH, UiO-66-NH_2, and **A6** all exhibit selectivity (i.e. a larger log(K_H)) for DMMP over toluene. However, the degree of selectivity, as estimated by the ΔK_H, is not equal for these three materials. In fact, UiO-66-NH_2 is more selective for DMMP than **A6** (ΔK_H = 22 vs. 16, respectively). While this result is initially surprising, it can be rationalized by the fact that **A6** has added aromatic groups as a result of functionalization, which likely increase the affinity of this material for toluene relative to UiO-66-NH_2. However, the most selective material tested is UiO-66-OH, highlighting the potential of this material given that it balances selectivity and affinity for DMMP without sacrificing either property.

Table 2—Comparison of Henry's Law binding constants for select sorbents with DMMP and toluene

Sample	Log(K_H) (DMMP)	Log(K_H) (Toluene)	ΔLog(K_H)	ΔK_H
UiO-66-OH	6.82 ± 0.01	5.37 ± 0.03	1.45	28
UiO-66-NH_2	6.30 ± 0.05	4.95 ± 0.04	1.35	22
A6	7.00 ± 0.02	5.79 ± 0.03	1.21	16

CONCLUSION

Through simple condensation reactions between the amine-functionalized MOF UiO-66-NH_2 and commercially-available benzaldehydes and benzoic acids, hydrogen-bond-acidic sorbent moieties were introduced into the UiO-66 framework. As a result, f-MOFs show decreased crystallinity and surface areas but still exhibit

reasonable porosities for adsorbent applications. In uptake studies with DMMP, these f-MOFs showed successful adsorption with noticeable impacts from the added sorbent groups. Excitingly, by normalizing uptake capacity to f-MOF surface area and correlating this property to Hammett substituent constants, structure-property relationships emerged that can guide future sorbent design. In the case of imine-functionalized MOFs, an expected trend was observed in which adding electron-deficient sorbent groups provides the best sorbent performance, in this case measured through uptake capacity. Unexpectedly, the opposite trend is observed for amide-functionalized MOFs, where electron-rich sorbent groups provide the best performance.

Ongoing work is focused on understanding these observed differences. In one such study, the binding affinities of these sorbents for DMMP were measured, although this investigation did not yield similar structure-property relationships as observed for uptake capacity. Instead, this investigation highlighted the beneficial impact of achieving high degrees of MOF functionalization, which increases the sorbent's affinity for DMMP. Future work will incorporate design principles elucidated in this study to generate improved sorbents, such as by increasing the pore size and surface area of the f-MOFs to reduce the negative impact of the added sorbent groups on overall uptake capacity.

ACKNOWLEDGMENTS

The authors would like to acknowledge the Office of Naval Research and the U.S. Naval Research Laboratory for funding this work. This project was supported in part by an appointment to the NRC Research Associateship Program at the U.S. Naval Research Laboratory in Washington, D.C., administered by the Fellowships Office of the National Academies of Sciences, Engineering, and Medicine. The authors would also like to acknowledge Courtney Roberts for discussions leading to early conceptions of this work; Thomas Sutto and Scott Mathews for assistance with x-ray diffraction studies; and Ken Grabowski for his support of this work.

REFERENCES

1 Bhuiyan, M. A. R.; Wang, L.; Shaid, A.; Shanks, R. A.; Ding, J. Advances and applications of chemical protective clothing system, *J. Ind. Text.* **2019**, *49*, 97–138.

2 DeCoste, J. B.; Peterson, G. W. Metal–organic frameworks for air purification of toxic chemicals, *Chem. Rev.* **2014**, *114*, 5695–5727.

3 Bobbitt, N. S.; Mendonca, M. L.; Howarth, A. J.; Islamoglu, T.; Hupp, J. T.; Farha, O. K.; Snurr, R. Q. Metal–organic frameworks for the removal of toxic industrial chemicals and chemical warfare agents, *Chem. Soc. Rev.* **2017**, *46*, 3357–3385.

4 *Organophosphorus insecticides: a general introduction*; International Programme on Chemical Safety; United Nationss Environment Programme, International Labour Organisation, World Health Organization: Geneva, 1986.

5 Kumar, P.; Kim, K.-H.; Deep, A. Recent advancements in sensing techniques based on functional materials for organophosphate pesticides, *Biosensors and Bioelectronics* **2015**, *70*, 469–481.

6 Woellner, M.; Hausdorf, S.; Klein, N.; Mueller, P.; Smith, M. W.; Kaskel, S. Adsorption and detection of hazardous trace gases by metal-organic frameworks, *Adv. Mater.*,**2018**, *30*, 1704679.

7 Kang, D. W.; Ju, S. E.; Kim, D. W.; Kang, M.; Kim, H.; Hong, C. S.; Emerging porous materials and their composites for NH_3 gas removal, *Adv. Sci.* **2020**, *7*, 2002142.

8 Islamoglu, T.; Chen, Z.; Wasson, M. C.; Buru, C. T.; Kirlikovali, K. O.; Afrin, U.; Mian, M. R.; Farha, O. K. Metal–organic frameworks against toxic chemicals, *Chem. Rev.* **2020**, *120*, 8130–8160.

9 Petit, C.; Karwacki, C.; Peterson, G.; Bandosz, T. J. Interactions of ammonia with the surface of microporous carbon impregnated with transition metal chlorides, *J. Phys. Chem. C* **2007**, *111*, 12705–12714.

10 Brown, P. N.; Jayson, G. G.; Thompson, G.; Wilkinson, M. C. Effect of ageing and moisture on the retention of hydrogen cyanide by impregnated activated charcoals, *Carbon* **1989**, *27*, 821–833.

11 Liu, Y.; Howarth, A. J.; Vermeulen, N. A.; Moon, S.-Y.; Hupp, J. T.; Farha, O. K. Catalytic degradation of chemical warfare agents and their simulants by metal-organic frameworks, *Coordin. Chem. Rev.* **2017**, *346*, 101–111.

12 Ni, Z.; Jerrell, J. P.; Cadwallader, K. R.; Masel, R. I. Metal−organic frameworks as adsorbents for trapping and preconcentration of organic phosphonates, *Anal. Chem.* **2007**, *79*, 1290–1293.

13 Britt, D.; Tranchemontagne, D.; Yaghi, O. M. Metal-organic frameworks with high capacity and selectivity for harmful gases, *Proc. Natl. Acad. Sci. U.S.A.* **2008**, ***105***, 11623–11627.

14 Montoro, C.; Linares, F.; Quartapelle Procopio, E.; Senkovska, I.; Kaskel, S.; Galli, S.; Masciocchi, N.; Barea, E.; Navarro, J. A. R. Capture of nerve agents and mustard gas analogues by hydrophobic robust MOF-5 type metal–organic frameworks, *J. Am. Chem. Soc.* **2011**, *133*, 11888–11891.

15 Moghadam, P. Z.; Fairen-Jimenez, D.; Snurr, R. Q. Efficient identification of hydrophobic MOFs: application in the capture of toxic industrial chemicals, *J. Mater. Chem. A* **2016**, *4*, 529–536.

16 Matito-Martos, I.; Moghadam, P. Z.; Li, A.; Colombo, V.; Navarro, J. A. R.; Calero, S.; Fairen-Jimenez, D. Discovery of an optimal porous crystalline material for the capture of chemical warfare agents, *Chem. Mater.* **2018**, *30*, 4571–4579.

17 Stassen, I.; Bueken, B.; Reinsch, H.; Oudenhoven, J. F. M.; Wouters, D.; Hajek, J.; Van Speybroeck, V.; Stock, N.; Vereecken, P. M.; Van Schaijk, R.; De Vos, D.; Ameloot, R. Towards metal–organic framework based field effect chemical sensors: UiO-66-NH_2 for nerve agent detection, *Chem. Sci.* **2016**, *7*, 5827–5832.

18 Cai, S.; Li, W.; Xu, P.; Xia, X.; Yu, H.; Zhang, S.; Li, X. *In situ* construction of metal–organic framework (MOF) UiO-66 film on Parylene-patterned resonant microcantilever for trace organophosphorus molecules detection, *Analyst* **2019**, *144*, 3729–3735.

19 O-Rear, J. G.; Griffith, J. R.; Reines, S. A. Some new fluorinated epoxies and polymeric derivatives, *J. Paint. Technol.*, **1971**, *43*, 113–119.

20 Ballantine, D. S.; Rose, S. L.; Grate, J. W.; Wohltjen, J. W. Correlation of surface acoustic wave device coating responses with solubility properties and chemical structure using pattern recognition, *Anal. Chem.*, **1986**, **58**, 3058–3066.

21 Grate, J. W.; Klusty, M.; McGill, R. A.; Abraham, M. H.; Whiting, G.; Andonian-Haftvan, J. The predominant role of swelling-induced modulus changes of the sorbent phase in determining the responses of polymer-coated surface acoustic wave vapor sensors, *Anal. Chem.* **1992**, *64*, 610–624.

22 Rebière, D.; Déjous, C.; Pistré, J.; Lipskier, J.-F.; Planade, R. Synthesis and evaluation of fluoropolyol isomers as saw microsensor coatings: role of humidity and temperature, *Sensor. and Actuat. B-Chem.* **1998**, *49*, 139–145.

23 McGill, R. A.; Nguyen, V. K.; Chung, R.; Shaffer, R. E.; DiLella, D.; Stepnowski, J. L.; Mlsna, T. E.; Venezky, D. L.; Dominguez, D. The "NRL-SAWRHINO": a nose for toxic gases, *Sensor. and Actuat. B-Chem* **2000**, *65*, 10–13.

24 McGill, R. A.; Mlsna, T. E.; Chung, R.; Nguyen, V. K.; Stepnowski, J. The design of functionalized silicone polymers for chemical sensor detection of nitroaromatic compounds. *Sensor. and Actuat. B-Chem* **2000**, *65*, 5–9.

25 Higgins, B. A.; Simonson, D. L.; Houser, E. J.; Kohl, J. G.; Mcgill, R. A. Synthesis and characterization of a hyperbranched hydrogen bond acidic carbosilane sorbent polymer: Carbosilane Sorbent Polymer, *J. Polym. Sci. A Polym. Chem.* **2010**, *48*, 3000–3009.

26 Roberts, C. A.; McGill, R. A. Bisphenol hypersorbents for enhanced detection of, or protection from, hazardous chemicals. US 11,325,100 B2, May 10, 2022.

27 Grissom, T. G.; Roberts, C. A.; Rodrigues, R.; Papantonakis, M. R.; Nguyen, V. K.; McGill, R. A. Sorbent interactions with hazardous chemicals and spectral detection strategies. In *Chemical, Biological, Radiological, Nuclear, and Explosives (CBRNE) Sensing XXI*, Proc. SPIE 11416, Online Only, 27 April, 2020; Guicheteau, J. A.; Howle, C. R.; 114160J.

28 Wang, Z.; Tanabe, K. K.; Cohen, S. M. Accessing postsynthetic modification in a series of metal-organic frameworks and the influence of framework topology on reactivity, *Inorg. Chem.* **2009**, *48*, 296–306.

29 Tanabe, K. K.; Cohen, S. M. Postsynthetic modification of metal–organic frameworks—a progress report, *Chem. Soc. Rev.* **2011**, *40*, 498–519.

30 Cohen, S. M. Postsynthetic methods for the functionalization of metal–organic frameworks, *Chem. Rev.* **2012**, *112*, 970–1000.

31 Islamoglu, T.; Goswami, S.; Li, Z.; Howarth, A. J.; Farha, O. K.; Hupp, J. T. Postsynthetic tuning of metal–organic frameworks for targeted applications, *Acc. Chem. Res.* **2017**, *50*, 805–813.

32 Ambroz, F.; Macdonald, T. J.; Martis, V.; Parkin, I. P.; Evaluation of the BET theory for the characterization of meso and microporous MOFs, *Small Method.* **2018**, *2*, 1800173.

33 Yin, Z.; Wan, S.; Yang, J.; Kurmoo, M.; Zeng, M.-H. Recent advances in post-synthetic modification of metal–organic frameworks: new types and tandem reactions, *Coordin. Chem. Rev.* **2019**, *378*, 500–512.

34 Mandal, S.; Natarajan, S.; Mani, P.; Pankajakshan, A. Post-synthetic modification of metal–organic frameworks toward applications, *Adv. Funct. Mater.* **2021**, *31*, 2006291.

35 Cavka, J. H.; Jakobsen, S.; Olsbye, U.; Guillou, N.; Lamberti, C.; Bordiga, S.; Lillerud, K. P. A new zirconium inorganic building brick forming metal organic frameworks with exceptional stability, *J. Am. Chem. Soc.* **2008**, *130*, 13850–13851.

36 Kandiah, M.; Nilsen, M. H.; Usseglio, S.; Jakobsen, S.; Olsbye, U.; Tilset, M.; Larabi, C.; Quadrelli, E. A.; Bonino, F.; Lillerud, K. P. Synthesis and stability of tagged UiO-66 Zr-MOFs, *Chem. Mater.* **2010**, *22*, 6632–6640.

37 Katz, M. J.; Brown, Z. J.; Colón, Y. J.; Siu, P. W.; Scheidt, K. A.; Snurr, R. Q.; Hupp, J. T.; Farha, O. K. A facile synthesis of UiO-66, UiO-67 and their derivatives, *Chem. Commun.* **2013**, *49*, 9449.

38 Biswas, S.; Van Der Voort, P. A general strategy for the synthesis of functionalised UiO-66 frameworks: characterisation, stability and CO_2 adsorption properties, *Eur. J. Inorg. Chem.* **2013**, *2013*, 2154–2160.

39 DeCoste, J. B.; Peterson, G. W.; Jasuja, H.; Glover, T. G.; Huang, Y.; Walton, K. S. Stability and degradation mechanisms of metal–organic frameworks containing the $Zr_6O_4(OH)_4$ secondary building unit, *J. Mater. Chem. A* **2013**, *1*, 5642.

40 Ingleson, M. J.; Barrio, J. P.; Guilbaud, J.-B.; Khimyak, Y. Z.; Rosseinsky, M. J. Framework functionalisation triggers metal complex binding, *Chem. Commun.* **2008**, 2680.

41 Doonan, C. J.; Morris, W.; Furukawa, H.; Yaghi, O. M. Isoreticular metalation of metal−organic frameworks, *J. Am. Chem. Soc.* **2009**, *131*, 9492–9493.

42 Tanabe, K. K.; Cohen, S. M. Engineering a metal-organic framework catalyst by using postsynthetic modification, *Angew. Chem. Int. Ed.* **2009**, *48*, 7424–7427.

43 Volkringer, C.; Cohen, S. M. Generating reactive MILs: isocyanate- and isothiocyanate-bearing MILs through postsynthetic modification, *Angew. Chem. Int. Ed.* **2010**, *49*, 4644–4648.

44 Kandiah, M.; Usseglio, S.; Svelle, S.; Olsbye, U.; Lillerud, K. P.; Tilset, M. Post-synthetic modification of the metal–organic framework compound UiO-66, *J. Mater. Chem.* **2010**, *20*, 9848.

45 Garibay, S. J.; Cohen, S. M. Isoreticular synthesis and modification of frameworks with the UiO-66 topology, *Chem. Commun.* **2010**, *46*, 7700.

46 Costa, J. S.; Gamez, P.; Black, C. A.; Roubeau, O.; Teat, S. J.; Reedijk, J. Chemical modification of a bridging ligand inside a metal–organic framework while maintaining the 3D structure, *Eur. J. Inorg. Chem.* **2008**, *2008*, 1551–1554.

47 Zhang, X.; Xia, T.; Jiang, K.; Cui, Y.; Yang Y.; Qian, G. Highly sensitive and selective detection of mercury (II) based on a zirconium metal-organic framework in aqueous media, *J. Solid State Chem.* **2017**, *253*, 277–281.

48 Brown, R. S.; Bennet, A. J.; Slebocka-Tilk, H. Recent perspectives concerning the mechanism of H_3O^+- and hydroxide-promoted amide hydrolysis, *Acc. Chem. Res.* **1992**, *25*, 481–488.

49 Chu, J.; Ke, F.-S.; Wang, Y.; Feng, X.; Chen, W.; Ai, X.; Yang, H.; Cao, Y. Facile and reversible digestion and regeneration of zirconium-based metal-organic frameworks, *Commun Chem* **2020**, *3*, 5.

50 Marreiros, J.; Caratelli, C.; Hajek, J.; Krajnc, A.; Fleury, G.; Bueken, B.; De Vos, D. E.; Mali, G.; Roeffaers, M. B. J.; Van Speybroeck, V.; Ameloot, R. Active role of methanol in post-synthetic linker exchange in the metal–organic framework UiO-66, *Chem. Mater.* **2019**, *31*, 1359–1369.

51 Brunauer, S.; Emmett, P. H.; Teller, E. Adsorption of gases in multimolecular layers, *J. Am. Chem. Soc.* **1938**, *60*, 309–319.

52 Thommes, M.; Kaneko, K.; Neimark, A. V.; Olivier, J. P.; Rodriguez-Reinoso, F.; Rouquerol, J.; Sing, K. S. W. Physisorption of gases, with special reference to the evaluation of surface area and pore size distribution (IUPAC Technical Report), *Pure Appl. Chem.* **2015**, *87*, 1051–1069.

53 Lykiema, J.; Sing, K. S. W.; Haber, J.; Kerker, M.; Wolfram, E.; Block, J. H.; Churaev, N. V.; Everett, D. H.; Hansen, R. S.; Haul, R. A. W.; Hightower, J. W.; Hunter, R. J. Reporting physisorption data for gas/solid systems with special reference to the determination of surface area and porosity, *Pure Appl. Chem.* **1985**, *57*, 603–619.

54 Walton, K. S.; Snurr, R. Q. Applicability of the BET method for determining surface areas of microporous metal−organic frameworks, *J. Am. Chem. Soc.* **2007**, *129*, 8552–8556.

55 Rouquerol, J.; Llewellyn, P.; Rouquerol, F. Is the BET equation applicable to microporous adsorbents? In *Studies in Surface Science and Catalysis*, Vol. 160; Elsevier, 2007; pp 49–56.

56 Kiani, S. S.; Faiz, Y.; Farooq, A.; Ahmad, M.; Irfan, N.; Nawaz, M.; Bibi, S. Synthesis and adsorption behavior of activated carbon impregnated with ASZM-TEDA for purification of contaminated air, *Diam. Relat. Mater*. **2020**, *108*, 107916.

57 Srivastava, A. K.; Shah, D.; Mahato, T. H.; Singh, B.; Saxena, A.; Verma, A. K.; Shrivastava, S.; Yadav, S. S.; Shrivastava, A. R.; Breakthrough behaviour of NBC canister against carbon tetrachloride: a simulant for chemical warfare agents, *Carbon Lett.* **2012**, *13*, 109–114.

58 Chen, Z.; Li, P.; Anderson, R.; Wang, X.; Zhang, X.; Robison, L.; Redfern, L. R.; Moribe, S.; Islamoglu, T.; Gómez-Gualdrón, D. A.; Yildirim, T.; Stoddart, J. F.; Farha, O. K. Balancing volumetric and gravimetric uptake in highly porous materials for clean energy, *Science* **2020**, *368*, 297–303.

59 Hammett, L. P. The effect of structure upon the reactions of organic compounds: benzene derivatives, *J. Am. Chem. Soc.* **1937**, *59*, 96–103.

60 Hansch, C.; Leo, A.; Taft, R. W. A survey of Hammett substituent constants and resonance and field parameters, *Chem. Rev.* **1991**, *91*, 165–195.

61 Lewis, M.; Bagwill, C.; Hardebeck, L. K. E.; Wireduaah, S. The use of Hammett constants to understand the non-covalent binding of aromatics, *Comput. Struct. Biotechnol. J.* **2012**, *1*, e201204004.

62 Charton, M. The application of the Hammett equation to ortho-substituted benzene reaction series, *Can. J. Chem.* **1960**, *38*, 2493–2499.

Appendix A

SUPPLEMENTAL DATA

INFRARED SPECTRA OF I1 AND A1

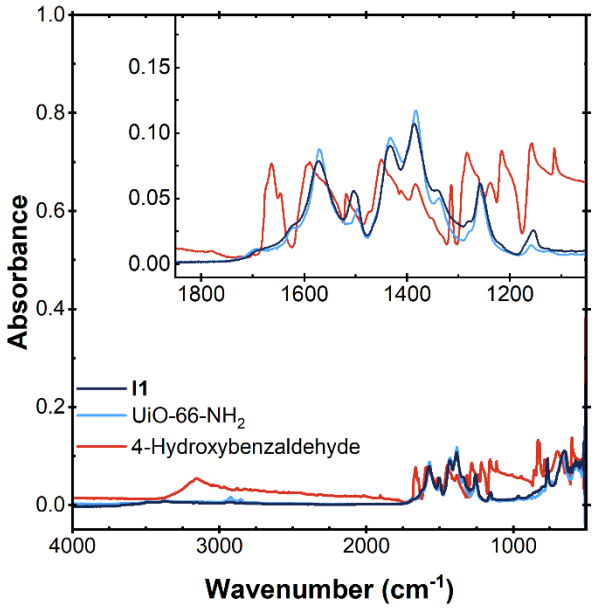

Fig. A1—IR spectrum of **I1** (dark blue), UiO-66-NH_2 (light blue), and 3-trifluoromethyl-4-hydroxybenzaldehyde (red)

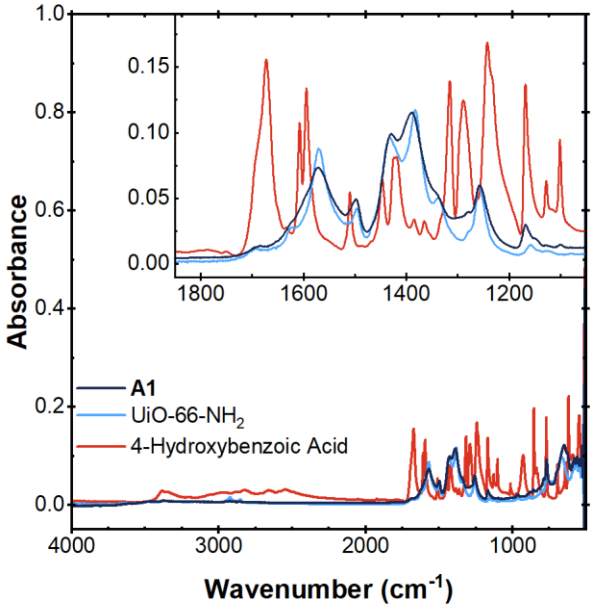

Fig. A2—IR spectrum of **A1** (dark blue), UiO-66-NH_2 (light blue), and 4-hydroxybenzoic acid (red)

POWEDER X-RAY DIFFRACTION OF I1 AND A1

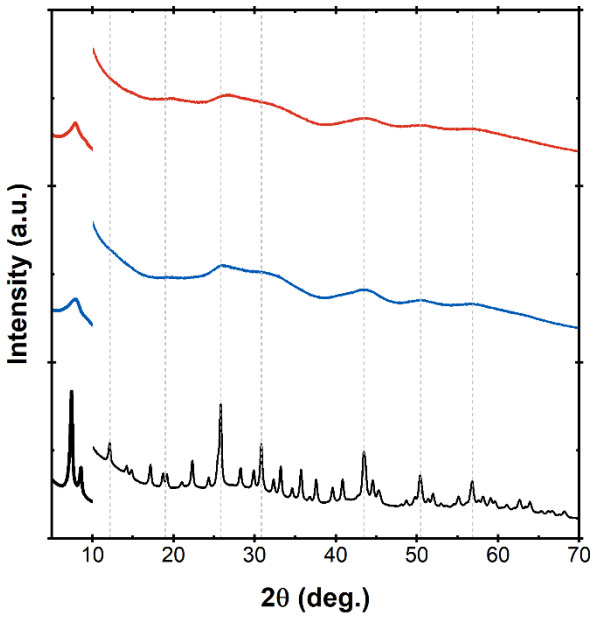

Fig. A3—Powder patterns of UiO-66-NH_2 (black), **I1** (blue), and **A1** (red), with grey lines highlighting similar features observed for each material. Data above 10° is magnified for clarity

NITROGEN GAS ADSORPTION DATA

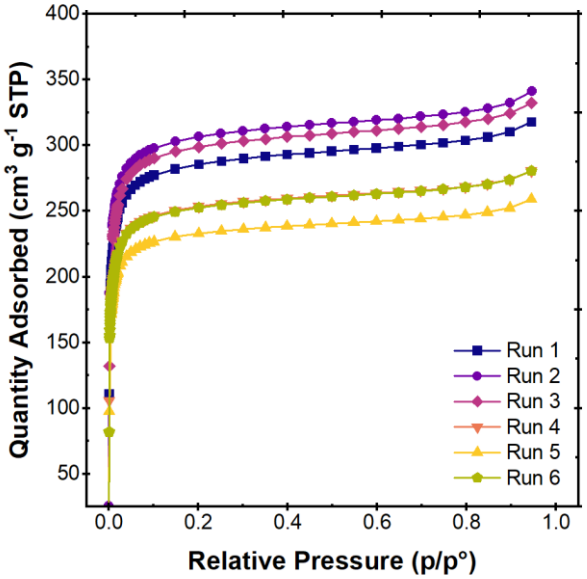

Fig. A4—Nitrogen gas adsorption data collected at 77K for UiO-66-NH_2

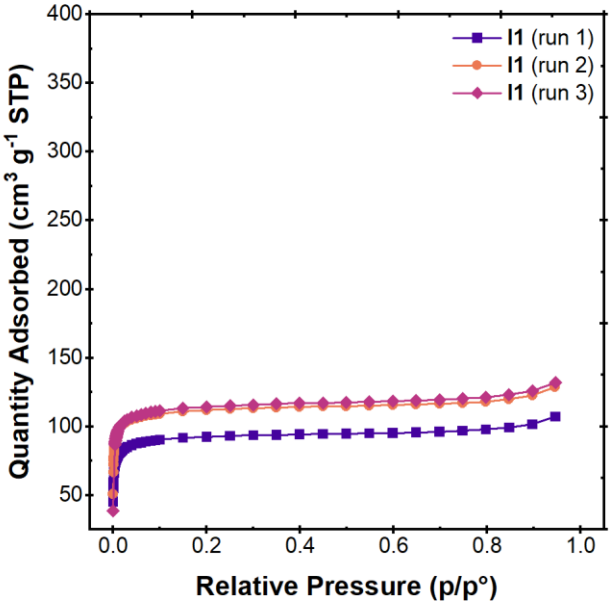

Fig. A5—Nitrogen gas adsorption data collected at 77K for **I1**

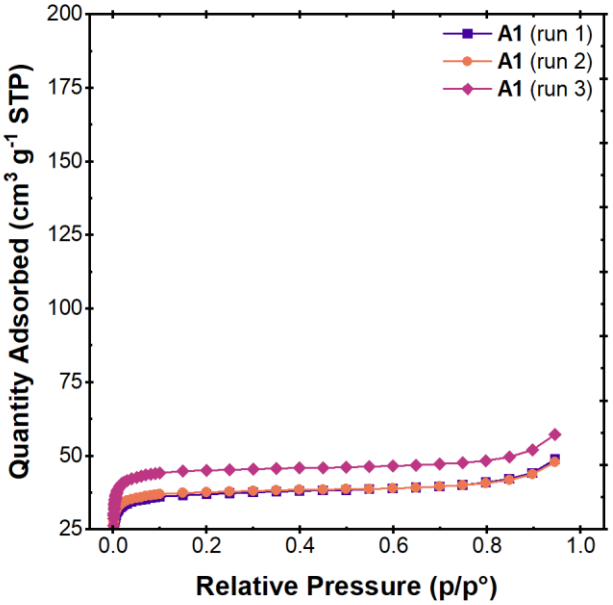

Fig. A6—Nitrogen gas adsorption data collected at 77K for **A1**

HENRY'S LAW DATA

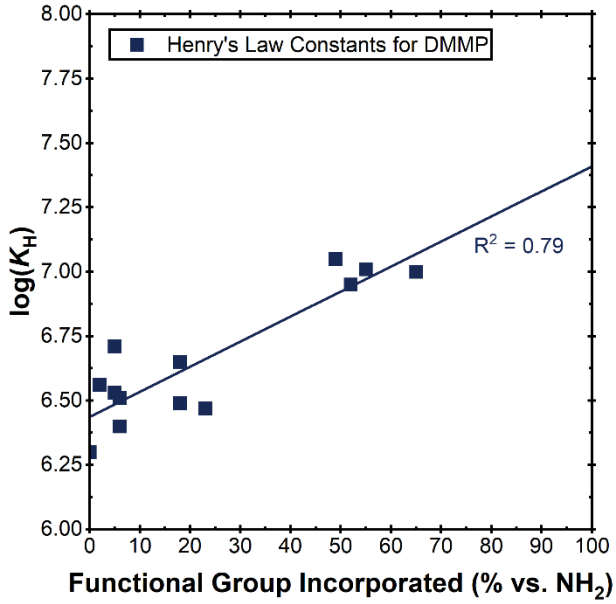

Fig. A7—Correlation of Henry's Law binding constants for DMMP with the degree of f-MOF functionalization